Angkasa Jurnal Ilmiah Bidang Teknologi
ISSN : 2085-9503 (Print)
ISSN : 2581-1355 (On Line)
Accredited Third Grade by Kemenristekdikti, Decree No: 10/C/C3/DT.05.00/2025
DOI : 10.28989/angkasa.v18i1.3503

Numerical Analysis of Mass Flow Rate Effect for 18650 Lithium-ion Battery Modules Thermal Management with Liquid Cooling System

Rainer Samuel Fourlando[1], James Julian[2]*, Fitri Wahyuni[3], Riki Hendra Purba[4], Fathin Muhammad Mahdhudhu[5], Elvi Armadani[6]
[1,2,3,4]Department of Mechanical Engineering, Universitas Pembangunan Nasional Veteran Jakarta, Indonesia
[5]Department of Naval Architecture, Universitas Pembangunan Nasional Veteran Jakarta, Indonesia
[6]Department of Industrial Engineering, Universitas Pembangunan Nasional Veteran Jakarta, Indonesia

Article Info

Article history:

Received October 05, 2025
Accepted December 01, 2025
Published February 27, 2026

Keywords:

Cold Plate,
Li-ion battery,
Liquid cooling,
Mass flow rate,
Mini-channel

ABSTRACT

Effective thermal management is critical for the safety and performance of lithium-ion batteries. This study numerically investigates a liquid cooling system with a mini-channel cold plate, focusing on how different coolant ṁ affect the thermal performance of an 18650 cylindrical lithium-ion battery module. Simulations were conducted using three mass flow rate (ṁ) 0.0001, 0.0003, and 0.0005 kg/s to evaluate their impact on maximum temperature (Tmax) and temperature difference (ΔT). Results show that increasing the ṁ significantly lowers the battery's maximum temperature. besides, increasing the ṁ will cause a higher pressure drop. All configurations successfully maintained excellent temperature uniformity, keeping the temperature difference well below the critical 5°C threshold. Therefore, this study confirms the system's effectiveness and highlights the necessity of optimizing (ṁ) based on the trade-off between thermal efficieny and pressure drop for designing reliable battery thermal management systems.

Corresponding Author:

James Julian,
Department of Mechanical Engineering,
Universitas Pembangunan Nasional Veteran Jakarta,
Jl. RS. Fatmawati Raya, Pd. Labu, Kec. Cilandak, Jakarta, Indonesia.
Email: *zames@upnvj.ac.id

1. INTRODUCTION

Batteries are the main source of energy and an irreplaceable part of electric vehicles, and their wide use is due to their advantages in reducing greenhouse gas emissions and petroleum consumption [1]. Li-ion batteries' benefits, such as their high specific energy, power density, extended cycle life, low self-discharge rate, and absence of memory effect, make them an ideal energy source for electric vehicles [1]. The electrochemical performance of lithium-ion batteries is strongly affected by temperature. High temperatures enhance lithium-ion migration and decrease internal resistance. While these conditions may foster certain benefits, they can also contribute to the battery's aging and potentially result in a more noticeable decrease in performance over time [2].

A comprehensive understanding of the effects of temperature variations on Li-ion batteries is essential [3]. Lowering the operating temperature of Li-ion batteries (LIBs) presents several challenges, including reduced lithium-ion transport, increased resistance, and decreased stability [4]. Lithium-ion batteries (LIBs) are particularly challenging to extinguish using conventional extinguishing agents [5]. Consequently, the problem of re-ignition remains a significant challenge, as a thermally runaway cell can remain hot enough to ignite residual fuel and even trigger thermal runaway in adjacent cells [6]. Although prismatics and pouch cells have a higher volumetric energy density, cylindrical cells offer distinct advantages in terms of thermal safety. The inherent spacing between cylindrical cells can act as a thermal barrier, potentially preventing the propagation of thermal runaway events [7]. The failures of LIBs may be triggered by exposure to an abnormal operating environment, There are several factors that may lead to potential challenges, including mechanical damage, external short circuits, overcharging, over discharging, and exposure to elevated temperatures. The fire generated by LIB is characterized by a notable heat release rate, a swift increase in temperature, and an extended period of elevated temperatures [5], [8].

Previous studies investigated a proposed innovative liquid cooling system for cylindrical lithium-ion battery modules. This system utilizes a variable contact surface with aluminum blocks to enhance efficiency and performance and the contact surface length dramatically improved temperature uniformity linearly. At an inlet velocity of 0.05 m/s, this approach decreased the temperature difference compared to a constant contact surface while also reducing system weight by 47% [9]. However, this study assumes that there is no contact thermal resistance and no thermal resistance that reduces the effectiveness of heat transfer. Another research numerically explored the influence of mechanical vibration on a thermal management system utilizing phase change materials (PCMs) for a single cylindrical battery. A low frequency of 10 Hz demonstrated a significant cooling effect, successfully lowering the maximum temperature by 28.05% compared to a non-vibrating system [10], [11]. Additionally, there is a limitation in the lack of experimental validation for the simulation results. Research that has been conducted investigates how varying the length of the condenser in a heat pipe array significantly influences the cooling efficiency of a battery thermal management system. Specifically, the design that a "wavy-like" effectively lowers the maximum cell temperature and the maximum temperature difference compared to a system utilizing a uniform condenser length [12]. The primary problem is the failure to consider unsteady air flow and thermal resistance, as the numerical model simplifies the heat pipe's internal physics by not simulating the phase-change process. Recent study optimized an air-cooling BTMS by designing a dual-inlet Y-shaped structure to replace traditional T-shaped designs. The research found that positioning the inlets at channels 3 and 7 was optimal, resulting in a 44.9% decrease in the maximum temperature difference compared to the T-shaped system, further enhancements with a stepped design reduced the maximum temperature and temperature difference by an additional 2.44% and 69.8%, respectively [13]. Nevertheless, the weakness lies in the limited experimental validation, as it only confirmed the CFD model's accuracy on a single cell, rather than a full-scale pack..

Prior research proposes a promising new design method for direct-contact liquid cooling plates, employing a multi-objective topology optimization approach. The optimized design drastically outperformed traditional rectangular plates, achieving a 52.54% reduction in pressure drop and a 65.65% reduction in thermal resistance. The optimal configuration featured a single inlet and two outlets, which demonstrated high thermal efficiency and low resistance [14]. However, controlling the system proved challenging. To achieve a flexible and efficient design for liquid cooling systems, it is recommended to maintain the temperature difference (ΔT) below 5°C and utilize topology optimization. The study is limited by its use of a 2D model stretched into 3D and the fabrication of an experimental prototype from low-conductivity polycarbonate. It can be concluded that liquid cooling effectively decreases the lowers temperature (Tmax) and also optimizes temperature uniformity (ΔT) under 5°C in 18650 cylindrical battery modules, which remains an unsolved problem. Based on the literature reviewed, the factors of efficiency and energy consumption in this liquid cooling technique are still rarely discussed, particularly in relation to mass flow rate ($\dot{m}$) as a parameter. By testing ($\dot{m}$) inside the cold plate, this research can be used as an essential parameter in determining the efficiency of the thermal management system. The Dominant mode of heat transfer in these battery cells is observed along the radial axis. Heat propagation occurs primarily in the radial direction, a phenomenon attributed to its moderate C-rate and to contributed internal heat generation.

2. METHOD

2.1. Lithium-ion Battery Model

This research focuses on a liquid cooling system designed for a cylindrical lithium-ion cell of the 18650 type. The battery, which is 18 mm in diameter and 65 mm in height, has a nominal capacity of 1.3 Ah. Figure 1 shows the dimensions of the battery model. The thermal characteristics of the battery pack model are considered homogeneous.

2.2. Mini-Channel Cold Plate Model

Power battery packs typically employ a modular structure designed to facilitate easy replacement and maintenance. To form a compact module, the battery module utilizes a geometric configuration in which the cells are arranged in two rows and a single column at the inlet. It is split into three columns inside and then reassembled into a single column at the end of the cold plate. The designed cooling system combines a mini-channel cold plate with a liquid cooling method, as illustrated in Figure 2, and is made of aluminum, a material proven to be lightweight and incredibly thermally conductive. This cold plate functions as a medium for heat transfer. The detailed properties of the materials are shown in Table 1.

Figure 1. Geometry details and dimensions of the Li-ion 18650 battery model

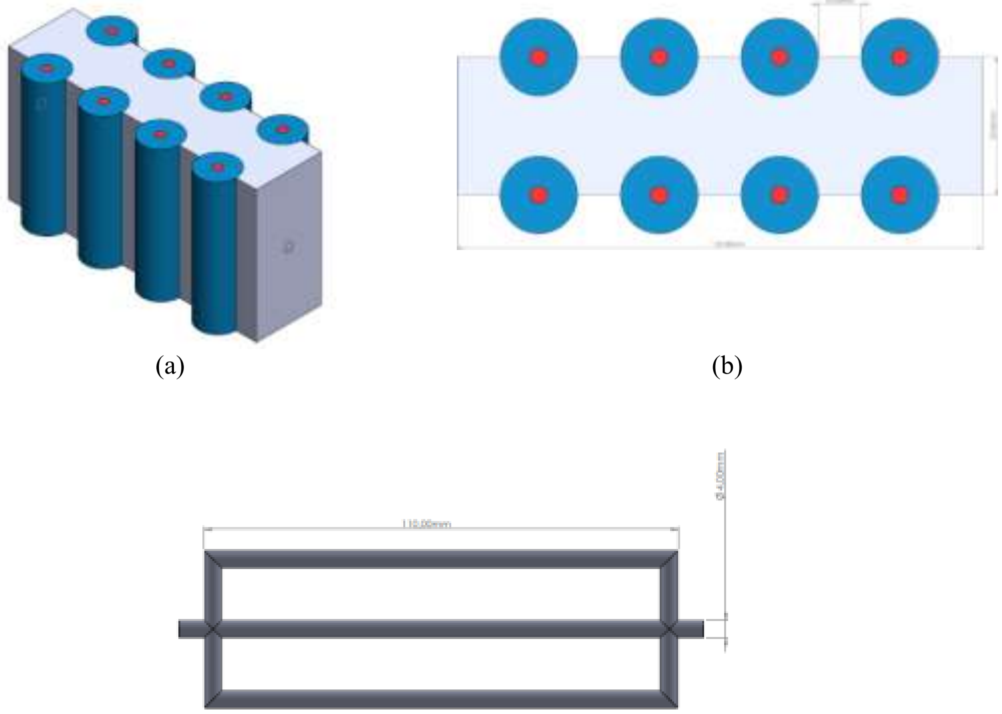

(a) (b)

(c)

Figure 2. The structural configuration of the mini-channel cold plate is intergrated into the liquid-cooled battery module

Table 1. The material properties conditions

Material	ρ (kg· m^{-3})	c (J·$\mathrm{kg}^{-1}\cdot\mathrm{k}^{-1}$)	k (W·$\mathrm{m}^{-1}\cdot\mathrm{k}^{-1}$)	µ (Pa·s)
Aluminium	2179	871	202.4	-
Battery	2534.26	15583	3.02	-
Water	998.2	4128	0.6	1.03x10^3

2.3. **Governing Equations**

Coolant fluid flow, as studied in this work, employs the Reynolds-averaged Navier-Stokes (RANS) technique, particularly in the mini-channel [15]. To ensure the fluid mass is maintained throughout the domain, the equations solved included Equation (1), the Mass Conservation (Continuity Equation). The equations (2) used to establish the law of conservation of momentum in fluid dynamics, while separate energy conservation equations determine the temperature fields in the fluid and solid domains, is calculated by equations (3). The heat source for the solid domain is defined by Equation (4), a model based on experimental thermal response data frequently used for homogeneous heat situations, defines the heat source for the solid domain. Therefore, inhomogeneous and unstable state heat transfer is taken into consideration by equation (5).

$$\frac{\partial \rho}{\partial t}+\frac{\partial}{\partial x_i}(\rho u_i)=0 \tag{1}$$

$$\frac{\partial}{\partial t}\left(\rho u_i\right)+\frac{\partial}{\partial x_i}(\rho u_i u_j)=-\frac{\partial \rho}{\partial x_i}+\frac{\partial}{\partial x_j}\left[\mu\left(\frac{\partial u_i}{\partial x_j}+\frac{\partial u_j}{\partial x_i}-\frac{2}{3}\delta_{ij}\frac{\partial u_i}{\partial x_i}\right)\right]+\frac{\partial}{\partial x_j}\left(-\rho\overline{u_i' u_j'}\right) \tag{2}$$

$$\rho C_p \frac{\partial T}{\partial t}=\lambda_x\frac{\partial^2 T}{\partial^2 x}+\lambda_y\frac{\partial^2 T}{\partial^2 y}+\lambda_z\frac{\partial^2 T}{\partial^2 z}+Q_{gen} \tag{3}$$

$$Q_{gen}(t)=\rho C_p\frac{\Delta T}{\Delta t} \tag{4}$$

$$Q_{gen(1-2)}(x,y,z,t)=Q_{gen(1-2)}(t)-\lambda\nabla^2 T_{(1-2)} \tag{5}$$

2.4. Mesh and boundary conditions

This study created an unstructured mesh in the shape of a tetrahedron. This was done to simplify complicated shapes, as shown in Figure 3a, the boundary conditions for the thermal computational model of the battery are respectfully presented in Figure 3b, the temperature of the entire solid domain, which consists of eight battery cells and an aluminum cold plate, is set consistently at 35°C from the start of the simulation to produce reliable transient simulation results. The fluid used in the simulation is water, so it's assumed to incompressible fluid. The water entered the system through a single inlet channel at a constant temperature of 25°C, split into three channels within, and was connected to a single outlet. Convection boundary conditions are applied to the exposed outer batteries surface with heat transfer coefficient is 5 W/(m^2·K) to represent the thermal interaction between the cold plate and battery. Table 2. presents the diameter of the channel and variations of $\dot{m}$ in detail. The impact of the input channels' geometrical configuration on the cooling system's thermal efficiency is evaluated numerically in this research. To achieve this, three modifications to the design were simulated by altering the inlet channel's diameter by 4 mm and to decreasing pressure drop, this study used a lower ($\dot{m}$) than the earlier research by varying the ($\dot{m}$) from 0.0005, 0.0003, and 0.0001 kg/s. Considering the axial gradient could be disregarded due to the comparatively low C-rate (2C), heat generation was applied as a volumetric heat source within each battery cell, with distribution concentrated on the radial gradient (core to surface).

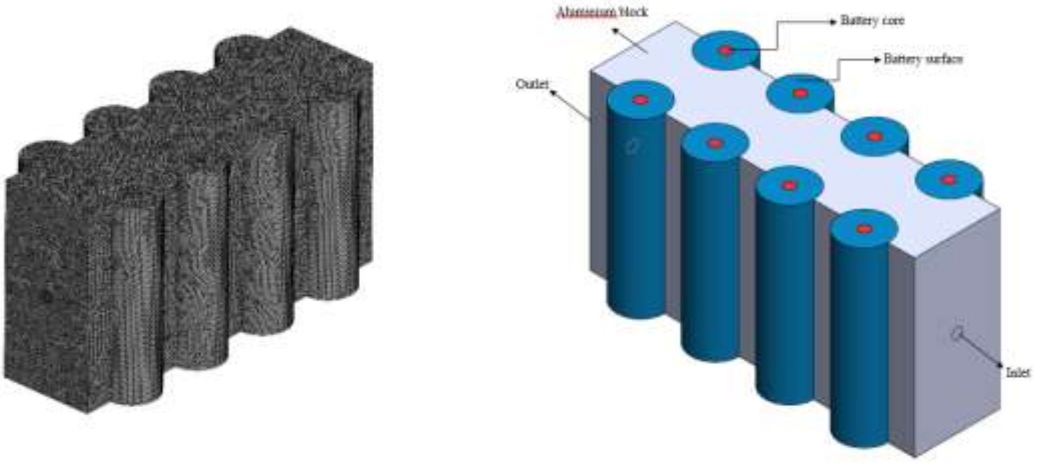

(a) (b)

Figure 3. Unstructured tetrahedron mesh configuration for the liquid cooling system (a) mesh, (b) boundary condition.

Table 2. Variation parameter and mass flow rate

Diameter Inlet (Ø)	Mass Flow Rate (kg/s)
0.004	0.0005
	0.0003
	0.0001

2.5. Non-dimensional parameter

In this research, equation (6) defines the Colburn factor (j) for evaluating heat transfer to indicate convective heat transfer performance. Moreover, to quantify the frictional resistance of the fluid flow in a channel, equation (7) is used for (f). Equation (8) explains (Re) is the Reynolds number, used to predict fluid flow pattern, equation (9) defines (Nu) The Nusselt number is a key measure that indicates the ratio of convective to conductive heat transfer across a boundary. Equation (10) represents (h_w) the heat transfer coefficient is a critical measure that quantifies the heat transfer rate to the surface area. To complete the analysis, equation (11) is the heat transfer (Q_l), which calculates the rate of heat absorbed by the coolant [16].

$$\mathrm{j} = \frac{\mathrm{Nu}}{\mathrm{Re} \cdot \mathrm{Pr}^{1/3}} \tag{6}$$

$$\mathrm{f} = \frac{2\Delta \mathrm{pDc}}{\rho_{\mathrm{l}} \mathrm{U}_{\mathrm{in}}^{2} \mathrm{L}} \tag{7}$$

$$\mathrm{Re} = \frac{\rho_{\mathrm{l}} \mathrm{U}_{\mathrm{in}} \mathrm{D}_{\mathrm{c}}}{\mu_{\mathrm{l}}} \tag{8}$$

$$\mathrm{Nu} = \frac{\mathrm{h}_{\mathrm{w}} \mathrm{D}_{\mathrm{c}}}{\lambda_{\mathrm{l}}} \tag{9}$$

$$\mathrm{h}_{\mathrm{w}} = \frac{\mathrm{Q}_{\mathrm{l}}}{\mathrm{A}_{\mathrm{c}}[\mathrm{T}_{\mathrm{bmax}} - (\mathrm{T}_{\mathrm{lin}} + \mathrm{T}_{\mathrm{lout}})/2]} \tag{10}$$

$$\mathrm{Q}_{\mathrm{l}} = \mathrm{c}_{\mathrm{pl}} \mathrm{m}_{\mathrm{l}} (\mathrm{T}_{\mathrm{lin}} - \mathrm{T}_{\mathrm{lout}}) \tag{11}$$

2.6. Mesh independence test

A grid sensitivity research was carried out. To account for mesh quality in relation to computing efficiency, the number of elements must also be further evaluated. Computes the error value in each mesh model using the grid convergence index. To calculate the error value in each mesh model, this researches use Roache's approach [17]. The mesh variations used are divided into three types: coarse, medium, and fine. Grid Convergence Index indices are discussed in equations (12) through (18) as a way to quantify the error and uncertainty involved in grid refinement research.

calculated by equations (12). The $\mathrm{GCI}_{\mathrm{fine}}$ calculate the error percentage from fine mesh elements through medium mesh elements, which is represented in equations (14). Furthermore, to calculate error percentage from medium mesh elements through coarse mesh element is calculated by $\mathrm{GCI}_{\mathrm{coarse}}$, as shown in equations (15). According to Roache's method in equations (17), the result that approximately one, able to confirms that a numerical simulation has reached the asymptotic range of convergence, which validates the solution and makes the Grid Convergence Index a reliable estimator of the discretization error. Deriving a numerical solution that accurately reflects the theoretical value at zero grid spacing is essential. This process is a crucial element of verification in computational simulations, providing an estimation of the exact solution to the governing equations, completely devoid of discretization error, this calculation is accomplished through equations (18).

In this analysis, we used ratios two, and the result is 3,506,106 fine grid elements for high modeling accuracy. This includes 860,695 coarse mesh elements for an overview and 1,750,227 medium mesh elements for balanced detail. The error metrics in Table 3 demonstrate the reliability of our mesh configurations and the effectiveness of our approach in capturing the system's intricacies.

$$\mathrm{r} = \frac{\mathrm{h}_2}{\mathrm{h}_1} \tag{12}$$

ISSN : 2085-9503 (Print), 2581-1355 (On Line)

$$\bar{p} = \frac{\ln\left(\frac{f_3 - f_2}{f_2 - f_1}\right)}{\ln(r)} \quad (13)$$

$$GCI_{fine} = \frac{F_s |\varepsilon|}{\left(r^{\bar{p}} - 1\right)} \quad (14)$$

$$GCI_{coarse} = \frac{F_s |\varepsilon| r^{\bar{p}}}{\left(r^{\bar{p}} - 1\right)} \quad (15)$$

$$\varepsilon = \frac{f_{n+1} - f_n}{f_n} \quad (16)$$

$$\frac{GCI_{coarse}}{GCI_{fine}} \approx 1 \quad (17)$$

$$fr_{h=0} = f_1 + \frac{\left(f_1 - f_2\right)}{\left(r^{\bar{p}} - 1\right)} \quad (18)$$

Table 3. Result of grid test

Mesh	**Difference of Temperature**	$\bar{p}$	**r**	GCI_{fine}	GCI_{coarse}	$f_{rh} = 0$	$\frac{GCI_{coarse}}{GCI_{fine} r^{\bar{p}}}$	**Error**
Fine	31.4164	2.770677226	2	0.015%	0.1032%	31.42021	1	0.01209%
Medium	31.3943							0.08250%
Coarse	31.2433							0.56300%

3. RESULTS AND DISCUSSION

The research begins with numerical validation based on confirmed experimental findings from earlier research by Nan Wang [18]. The thermal behavior of the single lithium-ion battery (LIB) model, operating at an initial ambient temperature of 35°C and subjected to a 2C discharge rate, is clearly illustrated in Figure 4. The maximum errors were 3.914% for the core and 3.474% for the surface, when compared to the experimental data. Furthermore, the temperature increase trend at each location matched the experimental conditions. A reference for models without cooling is subsequently provided by the validated numerical model.

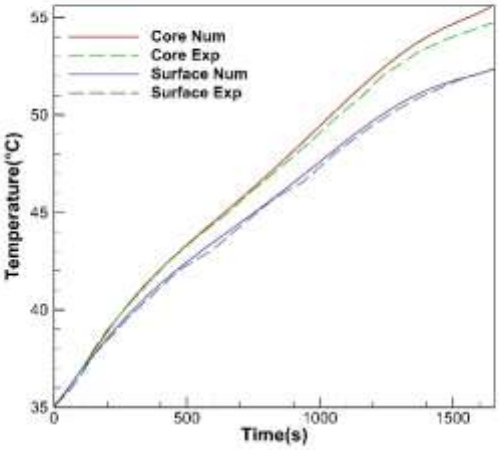

Figure 4. Comparison between experimental and numerical results of temperature response with discharge time on a single battery

Based on the curve shown in the Figure 4, it can be concluded that using a liquid cooling system has a very significant and crucial impact on battery thermal management, especially when compared to a scenario without cooling. Without a cooling system, the curve shows a rapid and uncontrolled increase in maximum temperature (T_{max}), exceeding 50∘°C at the end of the discharge process. This proves that a cooling system is essential to prevent excessive temperature increases that compromise battery performance and safety.

The lowest ṁ, 0.0001 kg/s, the battery's maximum temperature (T_{max}) experiences a slight increase in the first 300 seconds of the discharge process. After peaking at approximately 37°C, the temperature tends to stabilise and only decreases slightly until the end of the discharge period. This shows that although a low ṁ can control the temperature increase, its efficiency is not as optimal as that of higher rates. Cooling performance improved for a ṁ of 0.0003 kg/s. The maximum battery temperature showed a smaller initial spike than the lowest flow rate. After entering the 400 second, the T_{max} curve began to decline consistently until the end of the process.

Higher ṁ clearly demonstrate a significant cooling effect, effectively lowering the battery temperature after the initial peak.The improvement in cooling performance is most evident at the highest ṁ, 0.0005 kg/s. At this rate, the battery's initial temperature rise is minimal. The T_{max} curve peaks at the lowest temperature among the three scenarios, approximately 35.5°C, and thereafter shows the sharpest and most consistent temperature decrease. A higher ṁ clearly enhances heat dissipation from the battery, leading to a significantly lower overall operating temperature. Overall, the data in the Figure 5 confirm that an increase in ṁ is directly proportional to an increase in cooling performance and a decrease in the battery's maximum temperature. This analysis supports the design of an efficient cold plate, where the ṁ can be adjusted to achieve optimal thermal management.

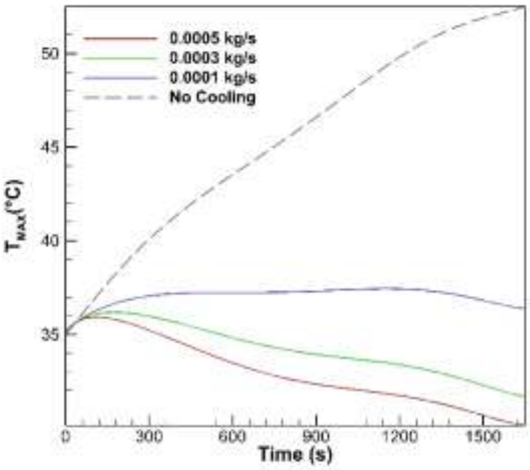

Figure 5. Maximum temperature curve for each variation of mass flow rate (kg/s) 0.0005, 0.0003, 0.0001.

All the mini-channel cold plate designs tested cooled well and helped heat escape more quickly. Each inlet geometry also lowered T_{max} and kept it safely under 37°C, frequently staying below 32°C until the simulation ended. The best result was achieved at a ṁ of 0.0005 kg/s, with a temperature of 32°C reached at 700 seconds. Temperature difference presented in Figure 6 are calculated radially between the core and surface of the 18650 battery cells at a discharge rate of 2C. These changes are in response to the challenges outlined in the introduction, which state that achieving temperature uniformity below the critical limit of 5 °C is necessary to prevent inconsistent degradation between cells. The ΔT value spikes sharply at the beginning of the cooling process (within the first 100-200 seconds) before decreasing significantly and stabilizing at a low level.

Figure 6 shows a quantitative assessment of thermal performance for each configuration. The highest ṁ 0.0005 causing the highest temperature difference 2.08°C in 104-126 seconds, and decreasing significantly until the end of simulation, at ṁ 0.0003 kg/s achieving the highest temperature difference at 1.73°C in 116-126 seconds, and significantly decrease the temperature after that, the lowest ṁ 0.0001 kg/s shows the best temperature uniformity compare to all configuration with 1.13°C highest temperature difference. The results highlight that the proposed liquid cooling system maintains temperature uniformity better than having no cooling.

All configurations are able to keep internal cell temperatures uniform. After the initial adjustment period, the temperature differences for all ṁ variations stay stable and below 1.5°C for the rest of the simulation. Even at the highest point, the temperature difference was less than 2.5°C, and this only happened briefly. These results indicate that this setup is most effective in maintaining low operational temperatures and ensuring even internal cell temperatures.

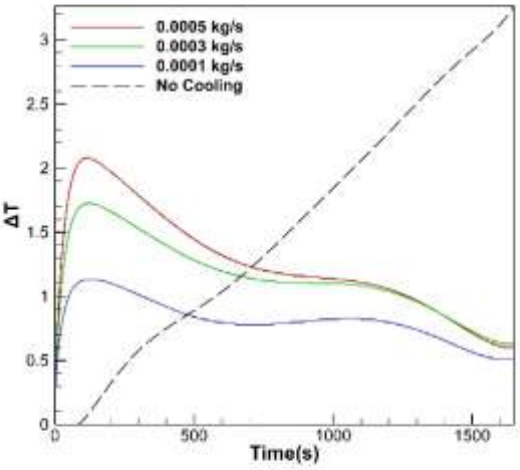

Figure 6. Evolution of temperature difference for each variation of mass flow rate (kg/s) 0.0005, 0.0003, 0.0001.

In this numerical analysis, although an increase in ṁ directly improves heat transfer performance, a comprehensive evaluation of the effectiveness of liquid cooling systems does not depend solely on flow rate. The cold plate configuration designed for the 18650 battery module must be analysed in depth to ensure that the increase in ṁ truly optimises heat transfer throughout the module. Variable performance at different ṁ, as reflected in differences in maximum temperature (T_{max}), indicates a trade-off between increased ṁ and thermal efficiency. Therefore, j factor will examine how ṁ interacts with cold plate design to achieve optimal thermal management, rather than simply increasing heat transfer.

This research uses J/F Factor to refine the analyzing between heat transfer performance and power consumption in the system, as illustrated in Figure 7. The analysis of varying the number of ṁ configurations revealed that there were no notable differences in the results. Despite altering the configurations, the outcomes remained consistent and did not exhibit any significant variations. The pump's power consumption has a substantial impact on the useful output power of the entire system. Beyond a specific flow rate, the pump's power consumption increases to a degree that further improvements in system efficiency become economically unjustifiable.

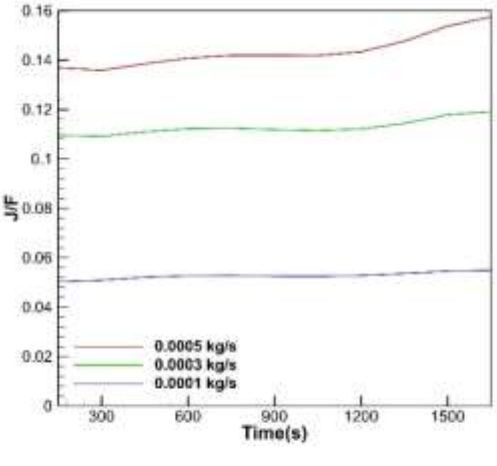

Figure 7. J/F factor difference for each variation of mass flow rate (kg/s) 0.0005, 0.0003, 0.0001.

The lowest ṁ 0.0001 value is 0.052. This value indicates adequate heat transfer capability at the lowest flow. Moreover, increasing ṁ to 0.0003 had some significant outcomes to 0.112. From all the configurations, 0.0005 ṁ shows the most effective J/F factor with a 0.143 value. According to Figure 7, the J/F value is increasing as the ṁ increase. Overall, these findings confirm that mass flow rate is an important factor in improving the thermal performance of cooling systems, although certain optimal limits must be taken into consideration.

Table 4 provides a valuable quantitative assessment of reduction in maximum temperature and ΔT each configuration, highlighting the significant advantages of the proposed liquid cooling system when compared to scenarios without cooling. All configurations exhibit commendable capabilities in maintaining uniform internal temperatures across each cell. Following the initial transient phase, variations in diameter demonstrate stability and consistency, with temperature differences (ΔT) holding steady below 1.5°C for the duration of the simulation. Even during peak conditions, the ΔT across all configurations remained below 2.2°C, and this occurred only temporarily.

The configuration with a ṁ of 0.0001 kg/s recorded the highest maximum temperature (Tmax) in battery four, reducing to 27.99%. However, as the ṁ increased to 0.0003 and 0.0005 kg/s, Tmax reduced to 30.42% and 30.90%, respectively. Additionally, Table 5 effectively quantifies the pressure drop in each configuration, revealing that increasing ṁ will cause a higher pressure drop. These findings underscore the superiority of this configuration in achieving both the lowest operational temperature and optimal uniformity within the internal cell temperatures.Figure 8 illustrates the configuration of the ṁ within the battery module. At varying ṁ, heat accumulates on its path to the outlet due to the slightly slower fluid flow. This phenomenon influences heat transfers in that area, as evidenced by the cross-section, which provides clarity on the radial heat distribution process.

Figure 8(a). visualise the battery pack with 0.0005 ṁ before reaching the minimum temperature, after 116 seconds, the temperature slowly decreases and stabilises at a low temperature of 29.62°C as the minimum temperature, the difference at the inlet through the outlet in this configuration is clearly displayed. Contour of 0.0003 ṁ before decreased to the minimum temperature is presented in Figure 8(b). In this configuration, the battery pack is visually more uniform, where the entire cold plate has almost the same temperature. This configuration reached 30.62°C at the minimum temperature after constantly decreased after 196 seconds. The 0.0001 configuration reached the minimum temperature at 34.71°C, Figure 8(c). shows that this configuration creates the most uniform temperature between the cold plate and batteries.

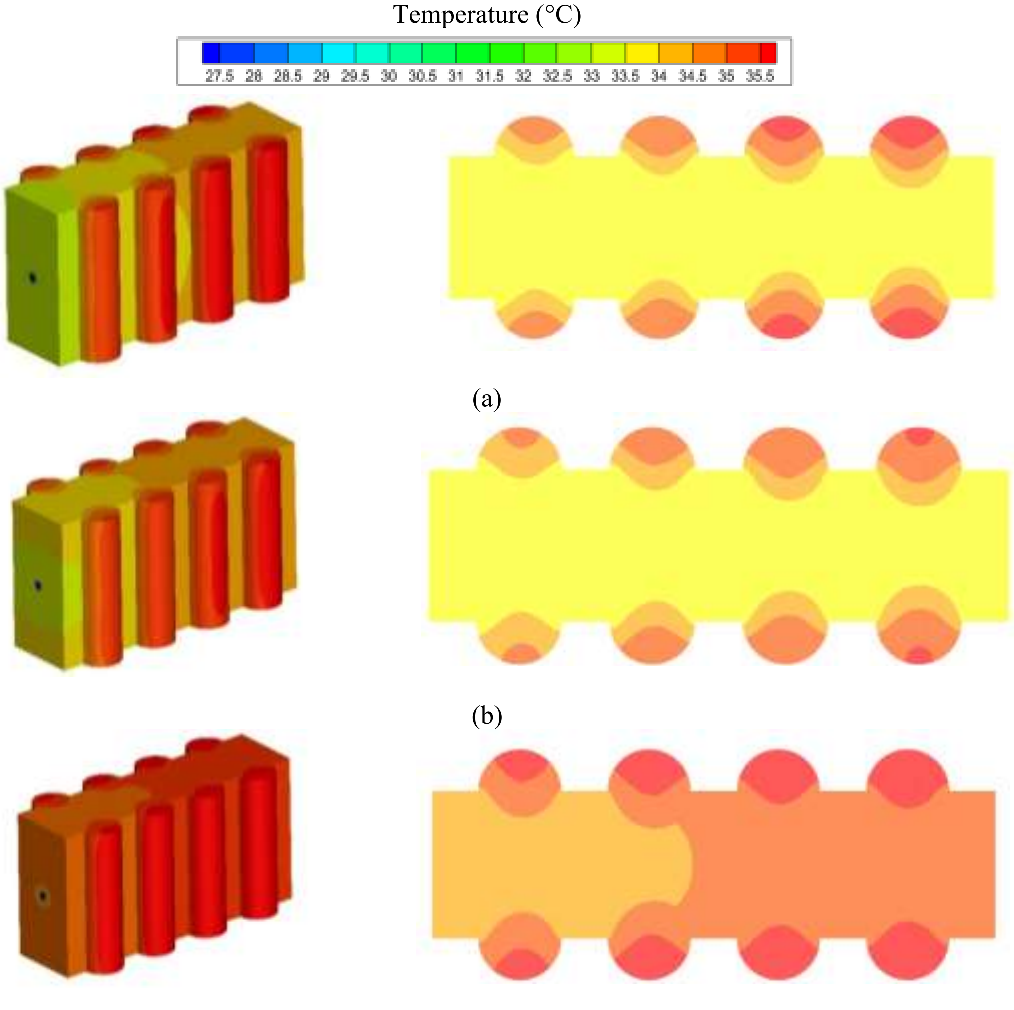

(a)

(b)

(c)

Figure 8. A comparison of thermal contours within the battery module for various mass flow rate (kg/s) (a) 0.005, (b) 0.0003, (c) 0.0001

Table 4. Comparison of Percentage reduction in maximum temperature and ΔT for each configuration.

	No Cooling		0.0001 kg/s		0.0003 kg/s		0.0005 kg/s	
Cell	T_{max}	ΔT	Temp. Reduction	ΔT	Temp. Reduction	ΔT	Temp. Reduction	ΔT
1	52°C	3.2647°C	29.06%	1.13°C	31.24%	1.73°C	31.42%	2.08°C
2			28.58%	1.02°C	30.93%	1.58°C	31.22%	1.89°C
3			28.19%	0.94°C	30.62%	1.46°C	31.02%	1.77°C
4			27.99%	0.88°C	30.41%	1.37°C	30.89%	1.68°C
5			29.06%	1.13°C	31.24%	1.73°C	31.41%	2.08°C
6			28.57%	1.02°C	30.93%	1.57°C	31.22%	1.89°C
7			28.19%	0.94°C	30.61%	1.47°C	31.02%	1.77°C
8			27.99%	0.88°C	30.42%	1.37°C	30.90%	1.67°C
Average			28.45%	0.9925°C	30.80%	1.535°C	31.14%	1.85375°C

Table 5. Pressure drop for each configuration.

$\dot{m}$	**0.0001 kg/s**	**0.0003 kg/s**	**0.0005 kg/s**
ΔP	1.000375354 Pa	3.451879527 Pa	6.426785380 Pa

4. CONCLUSIONS

Addressing the critical challenge of maintaining optimal operating temperatures and uniformity in lithium-ion battery modules, this numerical study successfully demonstrates that a mini-channel liquid cooling system effectively manages thermal performance. The results conclusively show a direct correlation between coolant $\dot{m}$ and thermal efficiency, where increasing the $\dot{m}$ from 0.0001 kg/s to 0.0005 kg/s significantly reduced the maximum battery temperature (T max) to as low as 32.81°C. Crucially, all tested configurations maintained the temperature difference (ΔT) well below the critical 5°C threshold, ensuring excellent cell uniformity. Based on these findings, future research should focus on optimizing the system for enhanced efficiency by investigating a wider range of $\dot{m}$ to identify an optimal balance between cooling performance and the required pumping power, and analyzing between heat transfer performance and power consumption in the system. Furthermore, studies could explore the geometric optimization of the mini-channel and cold plate design to maximize heat transfer and test the system's robustness under higher C-rate discharge conditions, thereby validating its performance under more extreme thermal loads. The application of such advanced studies would lead to the development of more energy-efficient, compact, and reliable thermal management systems, crucial for next-generation electric vehicles and high-power energy storage applications.

DAFTAR PUSTAKA (10 PT)

[1] P. Sun, R. Bisschop, H. Niu, and X. Huang, “A Review of Battery Fires in Electric Vehicles,” *Fire Technology 2020 56:4*, vol. 56, no. 4, pp. 1361–1410, Jan. 2020, doi: 10.1007/S10694-019-00944-3.

[2] S. Wang, J. Liu, and J. Y. S. Lin, “Failure analysis of ternary lithium-ion batteries throughout the entire life cycling at high temperature,” *Electrochim Acta*, vol. 508, p. 145238, Dec. 2024, doi: 10.1016/J.ELECTACTA.2024.145238.

[3] C. Villevieille, “The Numerous Materials Challenges Related to Post-Li-Ion Batteries,” *ACS Mater Lett*, vol. 7, no. 3, pp. 1057–1059, Mar. 2025, doi: 10.1021/ACSMATERIALSLETT.5C00285.

[4] J. Wang *et al.*, “Unlocking low temperature-resistant lithium metal batteries: Mechanisms, challenges, AI and functional electrolytes design,” *Materials Today*, vol. 88, pp. 979–1004, Sep. 2025, doi: 10.1016/J.MATTOD.2025.06.039.

[5] Y. Zhang, D. Kong, P. Ping, H. Zhao, X. Dai, and X. Chen, “Effect of a plate obstacle on fire behavior of 18650 lithium ion battery: An experimental study,” *J Energy Storage*, vol. 54, p. 105283, Oct. 2022, doi: 10.1016/J.EST.2022.105283.

[6] O. Mammacıoğlu and G. Coskun, “A new experimental approach to lithium-ion battery fires in electric vehicles: Investigation of fire behavior and effectiveness of extinguishing agents,” *Case Studies in Thermal Engineering*, vol. 73, p. 106554, Sep. 2025, doi: 10.1016/J.CSITE.2025.106554.

[7] F. Falcone, A. Giannotta, R. Ricco, and P. De Palma, “Thermal management systems for electric-vehicle Li-ion batteries: Review of safety issues and analysis of porous-media immersive cooling,” *Appl Therm Eng*, vol. 279, p. 127575, Nov. 2025, doi: 10.1016/J.APPLTHERMALENG.2025.127575.

[8] L. Zhang, K. Jin, J. Sun, and Q. Wang, “A Review of Fire-Extinguishing Agents and Fire Suppression Strategies for Lithium-Ion Batteries Fire,” *Fire Technology 2022 60:2*, vol. 60, no. 2, pp. 817–858, Jul. 2022, doi: 10.1007/S10694-022-01278-3.

[9] Z. Rao, Z. Qian, Y. Kuang, and Y. Li, “Thermal performance of liquid cooling based thermal management system for cylindrical lithium-ion battery module with variable contact surface,” *Appl Therm Eng*, vol. 123, pp. 1514–1522, Aug. 2017, doi: 10.1016/J.APPLTHERMALENG.2017.06.059.

[10] Z. Zhou, S. Chen, M. Luo, W. Du, Y. Wu, and Y. Yu, “Effect of mechanical vibration on phase change material based thermal management system for a cylindrical lithium-ion battery at high ambient temperature and high discharge rate,” *Int J Heat Mass Transf*, vol. 211, p. 124255, Sep. 2023, doi: 10.1016/J.IJHEATMASSTRANSFER.2023.124255.

[11] S. Rahmanian, H. Rahmanian-Koushkaki, and K. Hosseinzadeh, “Thermal management in high-power lithium-ion Batteries: Synergistic effects of phase change material thickness, graphene enhancers, and active cooling systems,” *Case Studies in Thermal Engineering*, vol. 74, p. 106771, Oct. 2025, doi: 10.1016/J.CSITE.2025.106771.

[12] O. M. Oyewola, O. S. Ismail, and A. A. Awonusi, “Effect of Heatpipe Array Condenser Section Length on Thermal Cooling of Li-Ion Batteries,” *Frontiers in Heat and Mass Transfer* , vol. 22, no. 2, pp. 475–490, 2024, doi: 10.32604/fhmt.2024.047714.

[13] L. Yang, X. Liao, K. Liu, X. Zhu, Y. Xu, and Y. Chao, “Optimization design of lithium-ion battery thermal management system based on Y-shaped air-cooling structure,” *Thermal Science and Engineering Progress*, vol. 66, p. 104062, Oct. 2025, doi: 10.1016/J.TSEP.2025.104062.

[14] J. Wu, X. Liu, N. Zheng, T. Zhou, and Z. Sun, “Design of direct contact liquid cooling systems for thermal management of lithium-ion batteries based on multi-objective topology optimization,” *J Energy Storage*, vol. 134, p. 118152, Oct. 2025, doi: 10.1016/J.EST.2025.118152.

[15] J. Julian, W. Iskandar, F. Wahyuni, and F. Ferdyanto, “COMPUTATIONAL FLUID DYNAMICS ANALYSIS BASED ON THE FLUID FLOW SEPARATION POINT ON THE UPPER SIDE OF THE NACA 0015 AIRFOIL WITH THE COEFFICIENT OF FRICTION,” *Media Mesin: Majalah Teknik Mesin*, vol. 23, no. 2, pp. 70–82, Jun. 2022, doi: 10.23917/MESIN.V23I2.18217.

[16] K. Ma, J. Wang, Q. Wang, and Q. Mao, “Numerical simulation of battery thermal management based on ring microchannel cold plate,” *International Journal of Thermal Sciences*, vol. 210, p. 109563, Apr. 2025, doi: 10.1016/J.IJTHERMALSCI.2024.109563.

[17] P. J. Roache, “Perspective: A Method for Uniform Reporting of Grid Refinement Studies,” *J Fluids Eng*, vol. 116, no. 3, pp. 405–413, Sep. 1994, doi: 10.1115/1.2910291.

[18] N. Wang, A. Chen, W. Zhao, R. Zhu, and B. Duan, “An online temperature estimation for cylindrical lithium-ion batteries based on simplified distribution electrical-thermal model,” *J Energy Storage*, vol. 55, p. 105326, Nov. 2022, doi: 10.1016/J.EST.2022.105326.